Lattice-dynamical calculation of phonon scattering at ideal Si–Ge interfaces

H. Zhao and J. B. Freund[a)]
Department of Theoretical and Applied Mechanics, University of Illinois at Urbana-Champaign, Urbana, Illinois 61801

(Received 22 July 2004; accepted 25 October 2004; published online 23 December 2004)

Detailed phonon scattering at an ideal Si–Ge interface is studied with a linear lattice dynamics model. Frequency dependent transmission coefficients indicate the significance of acoustic-optical phonon mode conversion at the interface. Applied to multiple interfaces, the method shows how the overall thermal resistance approaches a finite (Bloch mode) limit with the increasing number of interfaces in absence of other scattering mechanisms. The dependence of thermal resistance on the superlattice layer thickness is not significant even in the interface-scattering-only limit we study. We also assess errors incurred by the finite domain size and classical statistics in molecular dynamics simulations of interface thermal resistance. Results suggest that using 6×6 unit cells in the transverse directions, a tractable size for such simulations, will incur only a 5% error in the predicted thermal resistance. Similarly, the error due to the classical (Boltzmann) phonon distribution in molecular dynamics simulations is predicted to be less than 10% for temperatures above 300 K. © *2005 American Institute of Physics*. [DOI: 10.1063/1.1835565]

I. INTRODUCTION

It is well known that interfaces can play a dominant role in the overall thermal transport characteristics of structures whose length scale is less than the phonon mean free path. Superlattices are technologically interesting examples of such structures, with application in semiconductor lasers[1] and energy convertors.[2] In such applications, the mismatch of phonon dispersions between two different crystal lattices is a factor thought to cause significant phonon scattering at interfaces, reducing the overall device thermal conductivity. In this article, we focus on this mismatch mechanism though interface disorder, such as dislocations and defects, is thought to scatter phonons diffusively and may further reduce the thermal conductivity of superlattices or other structures. Experimental measurements of superlattice thermal conductivitiy[3–5] demonstrate that it can be reduced well beyond the standard Fourier law predictions. For example, the cross-plane thermal conductivity of a Si–Ge superlattice could be 90% smaller than the predictions based on bulk properties of pure Si and Ge.[3]

Theoretical modeling of interface dominant systems has been undertaken by using a Boltzmann transport equation (BTE) with acoustic mismatch or diffusive scattering models,[6,7] molecular dynamics (MD) simulations,[8,9] band gap models,[10] and linear lattice dynamics models.[11] If interfaces can be properly represented, BTE will be a useful tool for predicting thermal conductance in small structures,[12] bridging between larger scales where diffusion dominates and smaller scales where phonon transport is ballistic. However, both acoustic mismatch and diffusive scattering models currently used are relatively crude approximations for making quantitatively precise predictions. When the interfaces are periodic to a sufficient extent to be considered infinite, the band gap model is an appropriate approach in which the energy carriers are assumed only to be the coherent Bloch phonons. Simkin and Mahan[10] have applied the band gap model to explain the dependence of superlattice thermal conductivity on superlattice period. Here we mostly focus on a single interface between two semi-infinite leads, but also generalize the formulation to multiple interfaces to examine the approach to the Bloch limit. The direct simulation of an individual nearly single-frequency wave packet encountering an interface[13,14] can provide the details of single phonon scattering processes, but is excessively computationally expensive for phonons with small transverse wave numbers which are easily treated with the present lattice dynamics method.

Maris and Young[11] used such a lattice dynamics method to compute phonon reflection and transmission coefficients at an interface between two semi-infinite fcc lattices. Here we have generalized their model to study phonon scattering at an interface between two diamond structures, which allows us, for example, to assess the role of acoustic-optical phonon mode conversion at the interface. Molecular dynamics simulation of interface thermal resistance is an attractive way to incorporate the nonlinear mechanisms neglected by linear models such as ours, but is limited by its classical Boltzmann phonon distribution and finite transverse domain size. Thus we also use our method to estimate the impact of these limitations on molecular dynamics simulation results. The following sections detail our lattice dynamics (LD) method, briefly validate it against the wave packet results, and present our results.

II. FORMULATION

Crystalline Si and Ge are both fcc with a two-atom basis and slightly different unit cell sizes. However, in this study of Si–Ge interfaces, we consider an idealized model in which the Ge crystal shares the Si's unit cell size of $a=5.43$ Å, the

[a)]Electronic mail: jbfreund@uiuc.edu

actual lattice constant of Si. Any additional scattering due to the lattice mismatch for the actual $a=5.66$ Å of Ge is thereby neglected.

A. Phonon dispersion in pure crystals

We use the well accepted Stillinger–Weber potential[15] for the atomic interactions. Under the small displacement approximation (see the Appendix for the potential and linearization details), the lattice potential energy is

$$U=\tfrac{1}{2}\sum_{\mathbf{R},\mathbf{R}'}\mathbf{u}^T(\mathbf{R})\mathbf{D}(\mathbf{R}'-\mathbf{R})\mathbf{u}(\mathbf{R}'), \tag{1}$$

where $\mathbf{R}=(l/2,m/2,n/2)a$ are equilibrium fcc lattice sites with integers l, m, and n restricted such that $l+m+n$ is even. The six-dimensional vector $\mathbf{u}(\mathbf{R})$ denotes the displacements of the two atoms equilibrated at $\mathbf{R}$ and $\mathbf{R}+(a/4,a/4,a/4)$. The interaction matrix $\mathbf{D}(\mathbf{R}'-\mathbf{R})$ is thus 6×6 and defined

$$D_{ij}(\mathbf{R}'-\mathbf{R})=\frac{\partial^2 U}{\partial u_i(\mathbf{R})\,\partial u_j(\mathbf{R}')}, \tag{2}$$

with the obvious symmetry

$$\mathbf{D}(\mathbf{R})=\mathbf{D}^T(-\mathbf{R}). \tag{3}$$

In the Stillinger–Weber potential for crystalline Si or Ge as well as its linearized version, each fcc lattice site (containing two atoms) only interacts with its 12 nearest neighboring sites. So for each $\mathbf{R}$ in the summation of Eq. (1), only 13 $\mathbf{R}'$s (including $\mathbf{R}$ itself) yield nonzero $\mathbf{D}$ matrices.

From Eq. (1), the equation of motion is

$$M\frac{d^2\mathbf{u}(\mathbf{R},t)}{dt^2}=-\frac{\partial U}{\partial \mathbf{u}(\mathbf{R},t)}=-\sum_{\mathbf{R}'}\mathbf{D}(\mathbf{R}'-\mathbf{R})\mathbf{u}(\mathbf{R}',t), \tag{4}$$

where M is the atomic mass and we have used the symmetry property [Eq. (3)]. The wave solution of Eq. (4) is

$$\mathbf{u}(\mathbf{R},t)=\boldsymbol{\xi}\exp[i(\mathbf{k}\cdot\mathbf{R}-\omega t)], \tag{5}$$

where $\mathbf{k}$ is the wave number, ω is the wave frequency, and $\boldsymbol{\xi}$ is the six-dimensional polarization vector. Substitution of Eq. (5) into Eq. (4) yields

$$\hat{\mathbf{D}}(\mathbf{k})\boldsymbol{\xi}=M\omega^2\boldsymbol{\xi}, \tag{6}$$

where the dynamical matrix $\hat{\mathbf{D}}(\mathbf{k})$ is

$$\hat{\mathbf{D}}(\mathbf{k})=\sum_{\mathbf{R}}\mathbf{D}(\mathbf{R})\exp(i\mathbf{k}\cdot\mathbf{R}). \tag{7}$$

By Eq. (3), $\hat{\mathbf{D}}(\mathbf{k})$ is Hermitian for real valued wave numbers $\mathbf{k}$. For each $\mathbf{k}$, the eigensystem Eq. (6) has six solutions for ω^2 and $\boldsymbol{\xi}$, of which three $\omega^2-\boldsymbol{\xi}$ pairs are acoustic branches and the other three are optical.

B. Phonon group velocity

The phonon energy flow per unit area across a y-z plane from left to right is an integration over the first Brillouin zone

$$I=\frac{1}{(2\pi)^3}\int\sum_s \hbar\omega(\mathbf{k},s)n(\omega,T)v(\mathbf{k},s)H[v(\mathbf{k},s)]d\mathbf{k}, \tag{8}$$

where s is the phonon branch, n is the number of phonons of mode $(\mathbf{k},s)$, v is the x component of the phonon group velocity

$$v=\left.\frac{\partial\omega}{\partial k_x}\right|_{k_{y,z}}, \tag{9}$$

and H is the Heavyside function, which here restricts the integration to right-going phonons.

From Eq. (6), ω is an implicit function of $\mathbf{k}$ which makes the explicit evaluation of v seemingly difficult. However, an analytical expression for v can be derived by using a perturbation method. Equation (7) can be divided into three parts as

$$\hat{\mathbf{D}}(\mathbf{k})=\exp\left(-\frac{ik_xa}{2}\right)\hat{\mathbf{D}}_L+\hat{\mathbf{D}}_C+\exp\left(\frac{ik_xa}{2}\right)\hat{\mathbf{D}}_R, \tag{10}$$

where $\hat{\mathbf{D}}_L$, $\hat{\mathbf{D}}_C$, and $\hat{\mathbf{D}}_R$ are independent of k_x and represent a lattice site's interactions with atoms in planes to the left, coincident, and to the right of it, respectively. If there is no phonon branch degeneracy, both ω and $\boldsymbol{\xi}$ for a specific phonon branch are continuous functions of k_x. When a small perturbation δk_x is added to k_x, we have from Eq. (6) the differential relation

$$\delta\hat{\mathbf{D}}(\mathbf{k})\boldsymbol{\xi}+\hat{\mathbf{D}}(\mathbf{k})\delta\boldsymbol{\xi}=2M\omega\delta\omega\boldsymbol{\xi}+M\omega^2\delta\boldsymbol{\xi}, \tag{11}$$

where

$$\delta\hat{\mathbf{D}}(\mathbf{k})=\delta k_x\left[-\frac{ia}{2}\exp\left(-i\frac{k_xa}{2}\right)\hat{\mathbf{D}}_L+\frac{ia}{2}\exp\left(i\frac{k_xa}{2}\right)\hat{\mathbf{D}}_R\right]. \tag{12}$$

Taking the inner product of Eq. (11) with $\boldsymbol{\xi}$ and applying Eq. (6) gives

$$\boldsymbol{\xi}^H\delta\hat{\mathbf{D}}(\mathbf{k})\boldsymbol{\xi}=2M\omega\delta\omega|\boldsymbol{\xi}|^2, \tag{13}$$

where the superscript "H" indicates a complex-conjugate transpose. For real valued $\mathbf{k}$, the matrices $\hat{\mathbf{D}}_L$ and $\hat{\mathbf{D}}_R$ are complex conjugates of each other, so the x component of the phonon group velocity has the simple formula

$$v=\frac{\partial\omega}{\partial k_x}=\frac{\delta\omega}{\delta k_x}=-\frac{\mathrm{Im}[a\lambda\boldsymbol{\xi}^H\hat{\mathbf{D}}_R\boldsymbol{\xi}]}{2M\omega|\boldsymbol{\xi}|^2}, \tag{14}$$

where

$$\lambda=\exp\left(i\frac{k_xa}{2}\right). \tag{15}$$

When two different phonon branches α and β have the same frequency, we choose the two orthogonal polarization vectors that diagonalize $\delta\hat{\mathbf{D}}(\mathbf{k})$ to calculate v, as in a singular perturbation method.[16]

C. Reflection and transmission coefficients at an interface

We start by considering a case where the incident phonon has frequency ω and wave number $\mathbf{k}$ and travels rightward toward a y-z planar interface. To determine the reflection and transmission coefficients, it is essential to know the wave numbers and polarization vectors of the reflected and transmitted phonons. Since the system is harmonic and homogeneous in the y and z directions, all reflected and transmitted phonons must have the same ω, k_y, and k_z as the incoming phonon. We need to solve k_x and $\boldsymbol{\xi}$ from Eq. (6) that is

$$(\lambda^{-1}\hat{\mathbf{D}}_L + \hat{\mathbf{D}}_C + \lambda\hat{\mathbf{D}}_R)\boldsymbol{\xi} = M\omega^2\boldsymbol{\xi}, \tag{16}$$

where λ defined in Eq. (15) is a function of k_x only. Equation (16) is a nonlinear eigensystem for λ, but with the introduction of an auxiliary vector $\boldsymbol{\zeta}=\lambda\boldsymbol{\xi}$, it is transformed to

$$\begin{pmatrix} \hat{\mathbf{D}}_L & 0 \\ 0 & \mathbf{I} \end{pmatrix}\begin{pmatrix} \boldsymbol{\xi} \\ \boldsymbol{\zeta} \end{pmatrix} = \lambda\begin{pmatrix} -\hat{\mathbf{D}}_C + M\omega^2\mathbf{I} & -\hat{\mathbf{D}}_R \\ \mathbf{I} & 0 \end{pmatrix}\begin{pmatrix} \boldsymbol{\xi} \\ \boldsymbol{\zeta} \end{pmatrix}, \tag{17}$$

which is a generalized linear eigensystem. A similar equation was solved by Sanvito *et al.*[17] who transformed Eq. (17) to a standard eigenvalue problem in the form of $\mathbf{A}\boldsymbol{\xi}=\lambda^{-1}\boldsymbol{\xi}$ by inverting the matrix on the left-hand side. For singular $\hat{\mathbf{D}}_L$ as is the case for some modes of current interest, this approach fails, so we solve Eq. (17) directly as a generalized eigensystem. For each set of ω, k_y, and k_z, Eq. (16) has 12 k_x-$\boldsymbol{\xi}$ solutions, six of which are physically realistic and can be easily identified: a reflected phonon must have either negative $\mathrm{Im}[k_x]$ if k_x is complex so it decays in space, or it must have negative group velocity if k_x is real so it propagates away from the interface; the opposite holds for transmitted phonons. When $\hat{\mathbf{D}}_L$ or $\hat{\mathbf{D}}_R$ are singular, Eq. (17) gives spurious solutions of $|\lambda|=0$ or $|\lambda|=\infty$, which are inconsistent with the λ defined in Eq. (15). The corresponding atomic motions are physical but only exist in the lattice layer next to the dividing plane. These modes have either $\hat{\mathbf{D}}_L\boldsymbol{\xi}=0$ or $\hat{\mathbf{D}}_R\boldsymbol{\xi}=0$, so in this case lattice layers participating in these "surface" modes have zero influence on their neighbor layers to the right or to the left, respectively. Although these are not phonon modes, they are indispensable parts of the coherent vibrational motion of the composite lattice.

Consistent with the wave representation Eq. (5), atomic motions are

$$\mathbf{u}(\mathbf{R},t) = \boldsymbol{\xi}^{(i)}\exp\{i(\mathbf{k}^{(i)}\cdot\mathbf{R}-\omega t)\} + \sum_{s=1}^{6} r_s\boldsymbol{\xi}_s^{(r)}\exp\{i(\mathbf{k}_s^{(r)}\cdot\mathbf{R}-\omega t)\} \tag{18}$$

on the incoming phonon side of the interface and

$$\mathbf{u}(\mathbf{R},t) = \sum_{s=1}^{6} t_s\boldsymbol{\xi}_s^{(t)}\exp\{i[\mathbf{k}_s^{(t)}\cdot\mathbf{R}-\omega t]\} \tag{19}$$

on the other side, where the superscripts (i), (r), and (t) denote the incoming, reflected, and transmitted waves, respectively. Substitution of Eqs. (18) and (19) into the equation of motion for atoms at the interface yields a system of twelve linear equations which determines the reflected and transmitted wave amplitudes r_s and t_s.

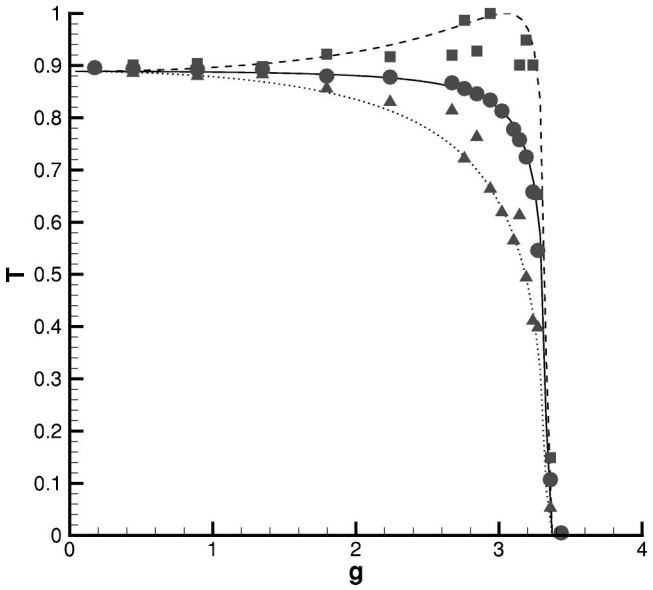

FIG. 1. Transmission coefficients $\mathcal{T}$ of transverse phonons in the [100] direction: solid line, ● average $\mathcal{T}$; dashed line, ■ maximal $\mathcal{T}$; dotted line, ▲ minimal $\mathcal{T}$. Lines are the present semianalytical results and symbols are from the wave packet computations of Schelling *et al.* (see Ref. 13).

Given a unit amplitude for the incident wave, the reflection coefficient is

$$\mathcal{R} = \frac{\sum_s |r_s|^2|v_s^{(r)}|}{|v^{(i)}|} \tag{20}$$

and the transmission coefficient is

$$\mathcal{T} = \frac{M_2\sum_s |t_s|^2|v_s^{(t)}|}{M_1|v^{(i)}|}, \tag{21}$$

where M_1 and M_2 are, respectively, atomic masses on the incoming and transmission sides of the interface. Energy conservation dictates that $\mathcal{T}+\mathcal{R}=1$.

III. RESULTS

A. Transmission of selected specific modes

Figure 1 shows the transmission coefficients for transverse [100] phonons. In this case, the two transverse phonon branches have the same frequencies and group velocities, so any linear combination of them is still a valid transverse polarization vector. The transmission coefficient $\mathcal{T}$ is then a quadratic function of the linear superposition coefficients

$$\mathcal{T} = \boldsymbol{\zeta}^H\mathbf{T}\boldsymbol{\zeta}, \tag{22}$$

where $\boldsymbol{\zeta}=(\alpha,\beta)^T$ is the linear combination coefficient vector and $\mathbf{T}$ is a 2 by 2 Hermitian matrix. Under the constraint $|\alpha|^2+|\beta|^2=1$, we find exactly the two polarization vectors that yield maximum and minimum $\mathcal{T}$ by diagonalizing $\mathbf{T}$. We note that all wave packet transmission coefficients computed by Schelling *et al.*[13] lie (to within plotting accuracy) between $\mathcal{T}_{\min}$ and $\mathcal{T}_{\max}$ computed by our lattice dynamics method (Fig. 1). It appears that the extrema found by Schelling *et al.* are

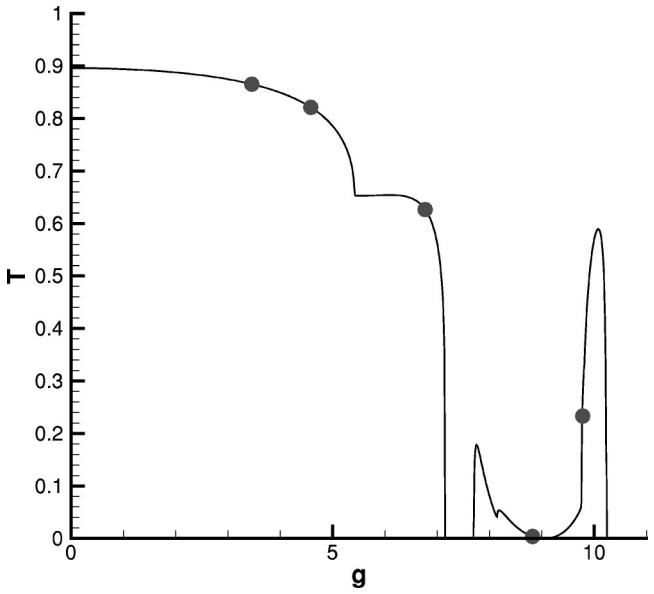

FIG. 2. Transmission coefficients $\mathcal{T}$ of the nondegenerate branch of phonons in the [111] direction: solid line—present method; ● wave packet method.

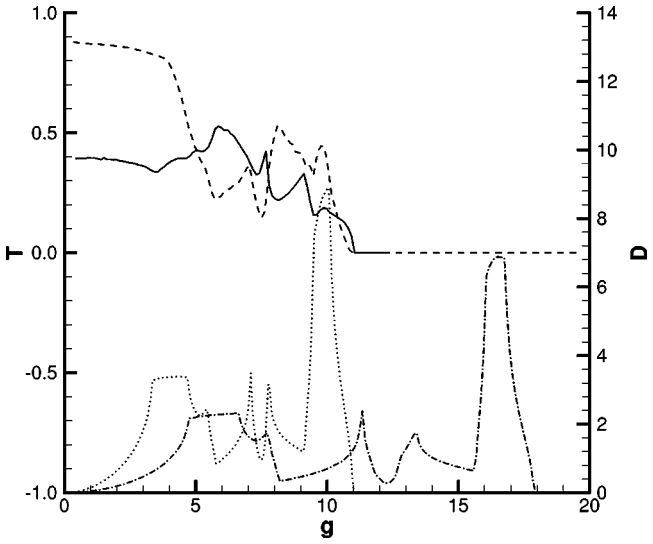

FIG. 3. Average transmission coefficient $\langle\mathcal{T}\rangle$ and DOS defined as the number of states per unit cell per THz: dashed line $\langle\mathcal{T}\rangle$ for Si→Ge; solid line $\langle\mathcal{T}\rangle$ for Ge→Si; dash-dot-dash line DOS in Si (scaled by $10^{12}a^{-3}$); dotted line—DOS in Ge.

for transverse polarization vectors only in a real linear subspace of the accessible complex linear space.

Figure 2 shows the specific transmission coefficients of [111] phonons at a Si–Ge interface. The incident phonon selected is the non-degenerate acoustic branch for Si. The agreement with our own wave packet simulation is perfect. The curve shows that the band gap between the acoustic and optical phonon modes of Ge causes total reflection at frequencies between $\gamma=7.15$ THz and $\gamma=7.69$ THz. The nonzero $\mathcal{T}$ at higher frequencies ($\gamma>7.69$ THz) results from phonon mode conversion from Si-acoustic to Ge-optical modes, which is discussed further in Sec. III B.

B. Average phonon transmission coefficients

The average transmission coefficient (weighted by phonon group velocity) at a specific angular frequency ω_0 is

$$\langle\mathcal{T}(\omega_0)\rangle = \frac{\int \sum_s \mathcal{T}(\mathbf{k},s)v(\mathbf{k},s)\delta[\omega_0-\omega(\mathbf{k},s)]H[v(\mathbf{k},s)]d\mathbf{k}}{\int \sum_s v(\mathbf{k},s)\delta[\omega_0-\omega(\mathbf{k},s)]H[v(\mathbf{k},s)]d\mathbf{k}}. \tag{23}$$

Figure 3 shows $\langle\mathcal{T}\rangle$ for both Si→Ge and Ge→Si phonon scatterings. At low frequencies, the values of $\langle\mathcal{T}\rangle$ for Ge→Si are lower than for Si→Ge. This is because the incoming phonons from Ge with nonzero k_y or k_z and small k_x have no matching Si phonon modes with the same k_y and k_z and real valued k_x since Si has a larger sound speed. Thus, these Ge incoming phonons are totally reflected, resulting in smaller values of $\langle\mathcal{T}\rangle$ for Ge→Si scattering. At higher frequencies, $\langle\mathcal{T}\rangle$ is correlated with the ratio between the density of states (DOS) of the outgoing and incoming crystal leads. This is most apparent at the steep drop of $\langle\mathcal{T}\rangle$ for Si→Ge near $\gamma=5$ THz, where the DOS in Ge decreases significantly while the DOS of Si is relatively unchanged with increasing γ. Likewise, $\langle\mathcal{T}\rangle$ for Ge→Si actually increases near $\gamma=5$ THz. The qualitative explanation for this correlation is that the ratio between the DOS's determines the relative populations of transmitted phonons to match the incoming ones.

We have also computed $\langle\mathcal{T}\rangle$ for Si→Ge scattering using a fcc lattice model. The spring constants between the nearest neighbors in the fcc model are estimated from the sound speed as done by Taumra *et al.*[18] A comparison of the results is shown in Fig. 4. Results from the two lattice models agree well when $\gamma<5$ THz. When $\gamma>5$ THz, the $\langle\mathcal{T}\rangle$ predicted by the simple fcc model drops as it must to zero, whereas the actual $\langle\mathcal{T}\rangle$ based on diamond structure remains nonzero until γ reaches the maximum supported frequency in Ge. Obviously, the nonzero $\langle\mathcal{T}\rangle$ at high frequencies comes from

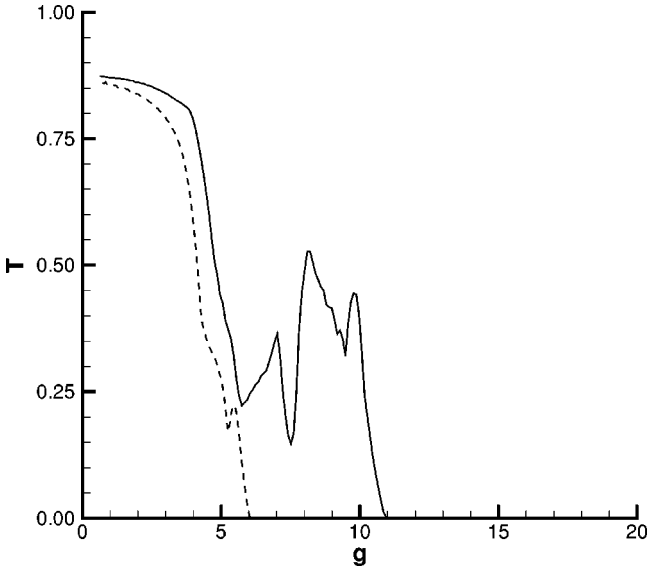

FIG. 4. Average transmission coefficient $\langle\mathcal{T}\rangle$ of Si→Ge scattering based on a solid line diamond cubic structure and a dashed line fcc lattice model.

acoustic-optical phonon mode conversion, which can only occur in actual diamond structures. As mentioned before, this mode conversion is also clear in Fig. 2.

C. Kapitza resistance

At thermal equilibrium, the energy flow per unit area across an interface is[19]

$$I_{1\to 2} = I_{2\to 1} = \frac{1}{(2\pi)^3}\int \sum_s \hbar\omega(\mathbf{k},s)n(\omega,T)v(\mathbf{k},s) \times \mathcal{T}(k,s)H[\pm v(\mathbf{k},s)]d\mathbf{k}. \quad (24)$$

The integration is restricted only to incident phonon modes by choosing $H[v(\mathbf{k},s)]$ for $I_{1\to 2}$ and $H[-v(\mathbf{k},s)]$ for $I_{2\to 1}$. The thermal boundary resistance κ is then

$$\kappa^{-1} = \frac{\partial I_{1\to 2}}{\partial T} = \frac{1}{(2\pi)^3}\int \sum_s \hbar\omega(\mathbf{k},s)\frac{\partial n(\omega,T)}{\partial T}v(\mathbf{k},s)\mathcal{T}(\mathbf{k},s)d\mathbf{k}, \quad (25)$$

where the phonon density $n(\omega,T)$ obeys the Bose–Einstein distribution

$$n = \frac{1}{\exp\left(\frac{\hbar\omega}{k_B T}\right) - 1}. \quad (26)$$

In choosing Eq. (26) as the phonon distribution, we have assumed that the distribution of incident phonons remains unchanged during the propagation from a hypothetical equilibrium phonon source to the interface, which is only strictly valid when the phonon mean free path is much longer than the distance between the phonon source and the interface. The temperature T in Eq. (25) is that of the bulk crystal lead as hypothetical phonon source. In MD simulations and in experiments, the temperatures are based on the local phonon distribution, which in general is not exactly the equilibrium bulk phonon distribution, but should be close enough for Eq. (25) to provide a very good estimate of κ. The definition of temperature in these circumstances is discussed in detail by Cahill *et al.*[20] Equation (25) also suggests the temperature dependence of Kapitza conductance κ^{-1} should be similar to that of the specific heat, and Fig. 5 confirms this.

As shown in Fig. 5, the value of κ^{-1} based on the Bose–Einstein distribution approaches that from the Boltzmann distribution as the temperature increases since the two distributions are, of course, identical at high temperatures. The difference is already within 10% at 300 K. Since the vibrational modes in MD simulations have Boltzmann distributions, we estimate that the phonon distribution correction to κ for Si–Ge interface is within 10% for MD simulations above 300 K and less than 1% for temperature above 1000 K. This provides some guidance for determining the temperature range within which classical MD simulation is suitable for such interfaces.

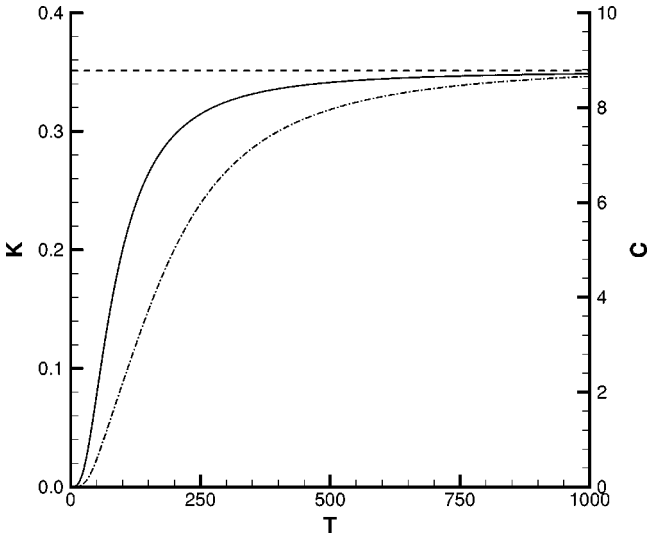

FIG. 5. Dependence of Kapitza conductance κ^{-1} on temperature: solid line—Bose–Einstein distribution; dashed line—Boltzmann distribution; dash-dot-dash line—specific heat of Si from linearized Stillinger–Weber potential.

Another limitation of MD is the size of the crystal that can be simulated. For an interface simulation, the transverse dimensions of the computational domain are usually limited to several unit cells and periodic boundary conditions are applied in these two directions. Such artificial boundary conditions reduce the allowed phonon wave numbers in transverse directions to a set of discrete numbers. To investigate this finite size effect, we have computed Kapitza conductance by summing only over discrete values of k_y and k_z, with cross section size varying from 2×2 to 11×11 unit cells. From the plots in Fig. 6, the conductance value is within 5% when the lattice has 6×6 unit cells in transverse directions, while the error is still as big as 30% when the transverse dimension is 4×4. Similar size dependence in MD simulations for pure Si crystals has been determined

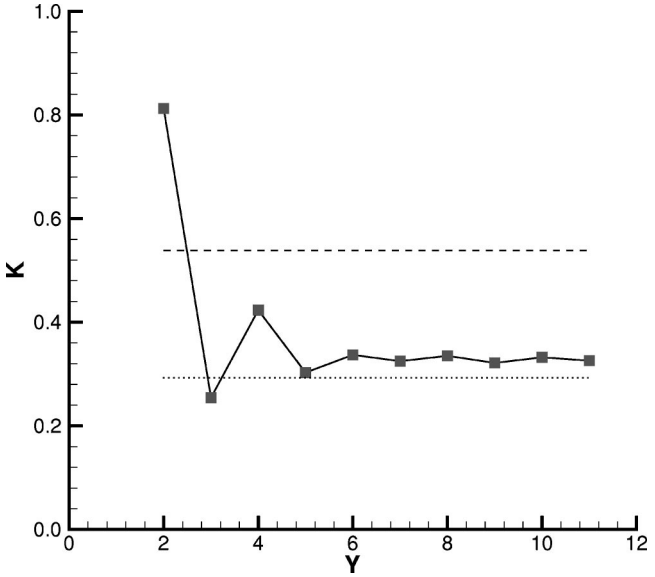

FIG. 6. Dependence of the Kapitza conductance κ^{-1} on the transverse domain size at 300 K: solid line—square cross section; dashed line—2×8 cross section; dotted line—3×5 cross section.

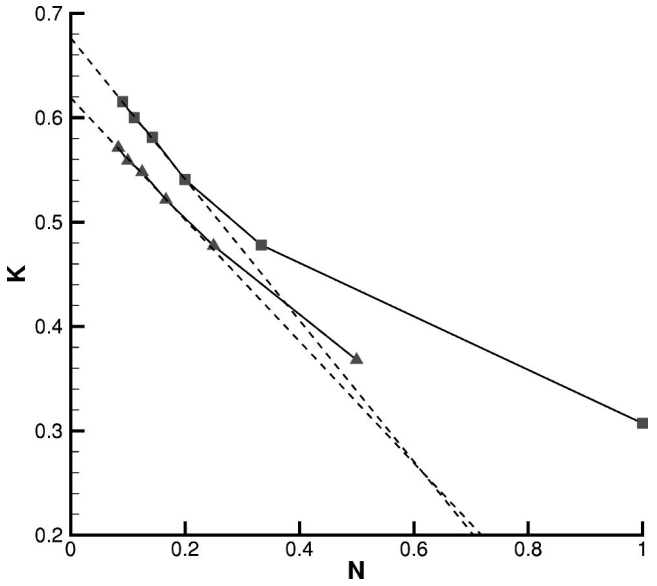

FIG. 7. Dependence of the thermal resistance κ on the increasing number of interfaces N at 300 K. Each layer is of six unit cells thick: ■ Si→Ge; ▲ Si→Si; dashed line—linear extrapolation.

empirically by Schelling *et al.*[21]. Interestingly, the 3×5 cross section gives a better result than 4×4, implying that a nonsquare cross section might provide a better sampling of wave number space.

D. Multiple interface scattering

Extending the lattice dynamics method to multiple interface scattering is straightforward and allows us to compute the overall thermal resistance of finite Si–Ge superlattices models. The dependence of the overall thermal resistance κ upon the number of interfaces N and the layer thickness is shown in Figs. 7 and 8. In Fig. 7, κ is almost a linear function of $1/N$ for $N>4$ and thus is expected to have a limiting value for $N\to\infty$. The curves for even versus odd numbers of layers are separated because they are of fundamentally different configurations. The former has Si in both leads and is designated Si→Si and the latter has Ge in the right lead and is designated Si→Ge. After passing several interfaces, the phonons will develop a coherent Bloch wave structure and will not be reflected further. This justifies the extrapolation to $1/N\to0$, which gives limiting values of $\kappa_{\mathrm{Si}\to\mathrm{Ge}}=6.77\times10^{-9}$ K m^2 W^{-1} and $\kappa_{\mathrm{Si}\to\mathrm{Si}}=6.19\times10^{-9}$ K m^2 W^{-1} and suggests that κ is within 10% of this Bloch wave limit after nine interfaces. Of course in real lattices, the phonon coherence length is finite due to the defects at the interfaces and aharmonic effects. However, the phonon mean free path in superlattices can cover several lattice layers, thus in BTE models, if we only use real valued phonon amplitudes as primitive variables without considering phases, such coherent structures will be missed and κ will be predicted to be almost linearly dependent on the number of interfaces, which is qualitatively incorrect for small N. The dependence on layer thickness is not significant. Figure 8 shows that κ varies by less than 10% for superlattice layer thicknesses from 2 to 12 atomic layers. Of course, this conclusion is only expected to hold when the total thickness is much smaller than the phonon mean free path when contributions to κ from other scattering mechanisms can be neglected.

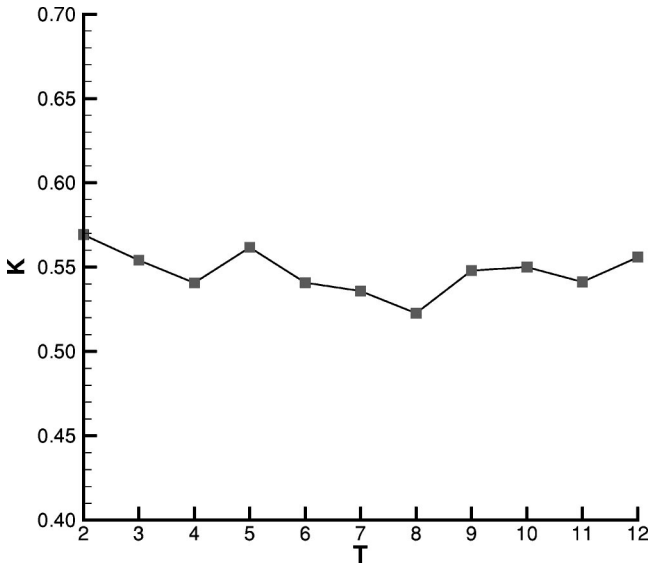

FIG. 8. Dependence of the Kapitza resistance κ on the superlattice layer thickness at 300 K for $N=5$ interfaces.

IV. CONCLUSIONS

Our linear lattice dynamics method has allowed us to analyze the phonon scattering processes at a perfectly matched interface between two diamond-cubic crystals, with parameters selected to model Si–Ge systems. We observe a correlation between the average transmission coefficient $\langle\mathcal{T}\rangle$ and the ratio between the density of states of the two crystal leads. Comparison to the simplified fcc lattice models of these diamond cubic crystals showed the significance of acoustic-optical phonon mode conversion for high frequency phonons. A possible application of the LD method is to provide boundary conditions for BTE models of mesoscale systems.

We also use the LD method to estimate the range of the validity of MD simulations, specifically with regard to the finite-size effect and the classical Boltzmann distribution of vibrational modes. We found that when the cross section of the computational domain is larger than 6×6 unit cells, the error due to the discrete sampling in wave number space is expected to be within 5%. Also, the error caused by phonon Boltzmann distribution in MD simulations is estimated to be within 10% at 300 K, and is less than 1% at 1000 K.

We also extended our computations to study phonon scatterings at multiple interfaces. For nine superlattice layers, we estimate that the net resistance is within 9% of its Bloch mode limit. Although for a superlattice structure which has many interfaces, a Bloch phonon description is a more natural choice, the LD method based on the bulk crystal phonons might afford greater flexibility for tailoring the interfaces to meet specific thermal design objectives.

ACKNOWLEDGMENTS

The authors wish to thank Gang Chen for introducing them to this area and for many helpful discussion and suggestions. They also gratefully acknowledge support from the National Science Foundation.

APPENDIX: LINEARIZATION OF STILLINGER–WEBER POTENTIAL

The Stillinger–Weber potential[15] for diamond structures consists of two parts: two-body interactions

$$v_2(r_{ij}) = \epsilon f_2(r_{ij}/\sigma), \tag{A1}$$

and three-body interactions

$$v_3(\mathbf{r}_i,\mathbf{r}_j,\mathbf{r}_k) = \epsilon f_3(\mathbf{r}_i/\sigma,\mathbf{r}_j/\sigma,\mathbf{r}_k/\sigma). \tag{A2}$$

The function f_2 in the two-body interaction

$$f_2(r) = \begin{cases} A(Br^{-p} - r^{-q})\exp[(r-a)^{-1}] & \text{if } r < a \\ 0 & \text{if } r \geqslant a, \end{cases} \tag{A3}$$

is spherically symmetric, thus its second derivatives at equilibrium positions are

$$\frac{\partial^2 v_2(r_{ij})}{\partial \mathbf{r}_i \partial \mathbf{r}_i} = \frac{\epsilon f_2''(r_{ij}/\sigma)}{\sigma^2} \frac{\mathbf{r}_{ij}}{r_{ij}} \otimes \frac{r_{ij}}{r_{ij}} \tag{A4}$$

and

$$\frac{\partial^2 v_2(r_{ij})}{\partial \mathbf{r}_i \partial \mathbf{r}_i} = -\frac{\partial^2 v_2(r_{ij})}{\partial \mathbf{r}_i \partial \mathbf{r}_j} = \frac{\partial^2 v_2(r_{ij})}{\partial \mathbf{r}_j \partial \mathbf{r}_j}, \tag{A5}$$

where $\mathbf{r}_{ij} = \mathbf{r}_i - \mathbf{r}_j$ and $f_2'(r_{ij}/\sigma) = 0$ was applied at equilibrium separations.

The three-body potential is

$$f_3(\mathbf{r}_i,\mathbf{r}_j,\mathbf{r}_k) = h(r_{ij},r_{ik},\theta_{jik}) + h(r_{ji},r_{jk},\theta_{ijk}) + h(r_{ki},r_{kj},\theta_{ikj}), \tag{A6}$$

where θ_{jik} is the angle between $\mathbf{r}_{ji}$ and $\mathbf{r}_{ki}$. The function h is

$$h(r_{ij},r_{ik},\theta_{jik}) = \lambda \exp[\gamma(r_{ij}-a)^{-1} + \gamma(r_{ik}-a)^{-1}] \times (\cos\theta_{jik} + 1/3)^2. \tag{A7}$$

Since the tetrahedral angle $\cos\theta = -1/3$ at equilibrium, we again have the simple expressions

$$\frac{\partial^2 h(\mathbf{r}_i,\mathbf{r}_j,\mathbf{r}_k)}{\partial \mathbf{r}_m \partial \mathbf{r}_n} = 2\lambda \exp[\gamma(r_{ij}-a)^{-1} + \gamma(r_{ik}-a)^{-1}] \times \frac{\partial \cos\theta_{jik}}{\partial \mathbf{r}_m} \otimes \frac{\partial \cos\theta_{jik}}{\partial \mathbf{r}_n}, \tag{A8}$$

where m and n are any two indexes in i, j, and k.

The parameters we used for bulk Si and Ge are $A = 7.049\,556\,277$, $B = 0.602\,224\,558\,4$, $p = 4$, $q = 0$, $a = 1.80$, $\gamma = 1.20$, $\sigma = 2.0951$ Å with $\lambda_{Si} = 21.0$, $\lambda_{Ge} = 31.0$, $\epsilon_{Si} = 3.473\,928 \times 10^{-19}$J, $\epsilon_{Ge} = 3.085 \times 10^{-19}$J. The Si–Ge values are linear combinations of these for pure crystals.

[1] T. E. Sale, IEE Proc.-J: Optoelectron. **142**, 37 (1995).
[2] L. D. Hicks and M. S. Dresselhaus, Phys. Rev. B **47**, 12727 (1993).
[3] S. M. Lee, D. G. Cahill, and R. Venkatasubramanian, Appl. Phys. Lett. **22**, 2957 (1997).
[4] T. Borca-Tasciuc *et al.*, Superlattices Microstruct. **28**, 199 (2000).
[5] A. Majumdar *et al.*, *IMECE* (ASME, New York, 2001).
[6] G. Chen, Phys. Rev. B **57**, 14958 (1998).
[7] G. Chen, Phys. Rev. Lett. **86**, 2297 (2001).
[8] B. C. Daly, H. J. Maris, K. Imamura, and S. Tamura, Phys. Rev. B **66**, 024301 (2002).
[9] B. C. Daly, H. J. Maris, Y. Tanaka, and S. Tamura, Phys. Rev. B **67**, 033308 (2003).
[10] M. V. Simkin and G. D. Mahan, Phys. Rev. Lett. **84**, 927 (2000).
[11] D. A. Young and H. J. Maris, Phys. Rev. B **40**, 3685 (1989).
[12] R. G. Yang and G. Chen, *IMECE* (ASME, New York, 2001).
[13] P. K. Schelling, S. R. Phillpot, and P. Keblinkski, Appl. Phys. Lett. **80** 2484 (2003).
[14] P. K. Schelling and S. R. Phillpot, J. Appl. Phys. **93**, 5377 (2003).
[15] F. H. Stillinger and T. A. Weber, Phys. Rev. B **31**, 5262 (1985).
[16] J. J. Sakurai and S. F. Tuan, *Modern Quantum Mechanics* (Addison-Wesley, New York 1994).
[17] S. Sanvito, C. J. Lambert, J. H. Jefferson, and A. M. Bratkovsky, Phys. Rev. B **59**, 11936 (1999).
[18] S. Tamura, Y. Tanaka, and H. J. Maris, Phys. Rev. B **60**, 2627 (1999).
[19] E. T. Swartz and R. O. Pohl, Rev. Mod. Phys. **61**, 605 (1989).
[20] D. G. Cahill, W. K. Ford, K. E. Goodson, G. D. Mahan, A. Majumdar, H. J. Maris, R. Merlin, and S. R. Phillpot, J. Appl. Phys. **93**, 793 (2003).
[21] P. K. Schelling, S. R. Phillpot, and P. Keblinski, Phys. Rev. B **65**, 144306 (2002).